Journal of Inorganic and Organometallic Polymers and Materials (2019) 29:258–268
https://doi.org/10.1007/s10904-018-0984-7

Phenanthrimidazole-Derivated Magnetic Silica Nanoparticles: Syntheses, Investigations of Morphology and Magnetic Properties

Aslihan Yilmaz Obali[1] · Ali Hussein Mustafa Al-Obaidi[1] · Halil Ismet Ucan[1]

Received: 22 August 2018 / Accepted: 25 September 2018 / Published online: 8 October 2018

Abstract
Novel phenanthrimidazole-derivated magnetic nanoparticles were synthesized originally. The chemical compositions of the hydroxy-, chloro-, carboxy-ended phenanthrimidazole derivatives were proved by FT-IR and ^{1}H-NMR spectroscopy and the pipe-like morphology was evaluated by SEM. The chemical compositions, morphologies and magnetic measurements of the magnetic nanoparticles were evaluated by FT-IR spectroscopy, TGA/DSC, XRD, TEM and VSM. The resulting products are spherical and aggregated by the magnetism of iron oxide, but dispersed individually in ethanol/water mixture.

Keywords Phenanthrimidazole · Magnetic · Nanoparticle · SPION · Imidazole · Magnetite · Maghemite · Silica

1 Introduction

In the last decade magnetic Fe_3O_4 nanoparticles have attracted spectacular interest due to their potential applications in biolabeling, magnetic immobilization, bioelectrocatalysis, magnetic carriers for drug delivery, magnetic resonance imaging contrast agents, tissue repair, immunoassay, detoxification of biological fluids, hyperthermia [1–4]. Many of these applications require the nanoparticles to be chemically stable, uniform in size and well dispersed in liquid medium. Due to the low toxic property of iron oxides, the most employed magnetic nanoparticles for biomedical applications have a magnetite or maghemite (Fe_3O_4 or γ-Fe_2O_3) core. Both magnetic forms of iron oxide safe for in vivo biomedical applications. Fe_3O_4 nanoparticles facilitate their use in biomedical applications, because of their magnetic property in the presence of an external magnet and non-magnetic property when the external magnet is removed [5–7].

To ensure magnetic nanoparticles' chemical stability and increase their dispersing ability, a coating material such as silica becomes crucial. In many applications, silica serves as an attractive coating material because of its stability, biocompatibility, ease of functionalization, and low cytotoxicity [8–10]. In this study we have coated Fe_3O_4 nanoparticles with 3-aminopropyl triethoxy silane (APTES) and (3-chloropropyl)dimethoxy silane (CPTES), separately. It is known that APTES (and CPTES) hydrolyzes in the presence of water and the silanol groups give condensation reaction with metal hydroxyl groups on the Fe_3O_4 nanoparticles' surfaces.

Phenanthrimidazoles are important heterocycles in medicinal chemistry, material sciences and biological sciences [11–16]. They are well-known for their ability to form many useful metal complexes and display a biological activity for drug discovery studies because of their antiviral, anti-ulcer, anti-hypertension, and anticancer antifungal properties. Therefore, the synthesis of phenanthrimidazoles from phenanthraquinone and an aromatic aldehyde, has a big interest nowadays [17–21].

Three heterocyclic phenanthrimidazole derivatives have been synthesized by the condensation reaction of 1,10-phenanthroline-5,6-dione with aromatic aldehydes as 4-hydroxybenzaldehyde (and 4-carboxybenzaldehyde) in the presence of ammonium acetate in glacial acetic acid medium. The chloro-substituted phenanthrimidazole compound was synthesized by the reaction of (imidazo[4,5-f][1,10]phenanthroline-2-yl)phenol and 1-bromo-3-chloropropane in DMF solution. Then they were reacted with silica-coated magnetic Fe_3O_4 nanoparticles to gain magnetic properties.

✉ Aslihan Yilmaz Obali
aslihanyilmaz@selcuk.edu.tr

[1] Department of Chemistry, Science Faculty, Selcuk University, Konya, Turkey

2 Experimental Section

2.1 Materials and Methods

1,10-Phenanthroline-5,6-dione [22], 4-(1*H*-imidazo[4,5-f][1,10]phenanthroline-2-yl)phenol [23] and 2-(4-carboxyphenyl)imidazo[4,5-f][1,10]phenanthroline [24] were synthesized by the literature methods. Other compounds were synthesized originally. All the chemicals were of reagent grade used without further purifications. Iron(III) chloride ($FeCl_3$, ≥ 99%), iron(II) sulphate heptahydrate ($FeSO_4{\cdot}7H_2O$, ≥ 99%) were obtained from Aldrich while sodium hydroxide (NaOH, ≥ 99%) and hydrochloric acid (HCl, ≥ 37%) from Merck. (3-aminopropyl)triethoxysilane (APTES) and (3-chloropropyl)dimethoxysilanol (CPTES) were purchased from Sigma-Aldrich.

2.2 Instruments

^{1}H-NMR spectra were recorded on Varian 400-MHz Spectrometer. FT-IR spectra were taken by a Perkin Elmer Spectrum 100 FT-IR spectrometer. Melting points were determined by Büchi Melting Point B-540 instrument. Elemental analyses were carried out using a LECO-CHNS-932 elemental analyser. The size and shape of the nanoparticles were determined by Transmission electron microscopy, JEOL JEM-2100 (UHR). Scanning electron microscopy images were obtained using a Zeiss LS-10 field emission SEM instrument. Bruker D8 Advance X-ray Diffractometer was used for all XRD measurements. The VSM hysteresis measurements were performed using Cryogenic Limited PPMS instrument. Magnetic susceptibilities of metal complexes were determined using a Sheerwood Scientific MX Gouy magnetic susceptibility apparatus using the Gouy method with $Hg[Co(SCN)_4]$ as calibrant. All aqueous solutions were prepared with deionized water that passed through a Millipore milli Q Plus water purification system.

2.3 Preparations of Phenanthrimidazole-Derivated Molecules

2.3.1 1,10-Phenantroline-5,6-dione

Phenanthroline (0.54 g, 3 mmol) was added into a solution of 60% sulfuric acid (7 mL), and stirred until dissolved. After solid compound was dissolved, potassium bromate (0.55 g, 3.3 mmol) was added in batches over a period of half an hour. The mixture was stirred at room temperature for 20 h. Then, the mixture was poured over ice and was carefully neutralized to pH:7 using a saturated solution of sodiumhydroxide. The solution was then filtered, extracted with dichloromethane and evaporated to dryness. The crude product was recrystallized from methanol to provide the desired product in 85–90%. FT-IR (cm^{-1}): 1683 (C=O), 1573, 1557, 1455, 1412, 1290, 1202, 1112, 922, 813, 736. 1H NMR ($CDCl_3$): δ = 7.62 (d, 2H), 8.53 (dd, 2H), 7.40 (dd, 2H), 9.15 (dd, 2H).

2.3.2 4-(1*H*-Imidazo[4,5-f][1,10]phenanthroline-2-yl) phenol, (Phen-OH)

1,10-Phenanthroline-5,6-dione (0.1 g, 0.46 mmol) and ammonium acetate (0.58 g, 13.3 mmol) were dissolved in 10 mL of hot glacial acetic acid. While the mixture was stirred, a solution of 4-hydroxybenzaldehyde (0.056 g, 0.46 mmol) in 10 mL of glacial acetic acid was added dropwise to the mixture. Then the mixture was heated to 90 °C for 3 h and was then poured in 200 mL of water. The solution was neutralized with ammonia to pH:7 and was then cooled to room temperature. The precipitate was filtered off and washed with large portions of water. The product was dried for 48 h in vacuo at 50 °C. FT-IR (cm^{-1}): 3392 (O–H), 3165 (N–H), 2998 (CH_2), 1659 (C=N), 1230 (C–O–C), 736 (CH, pyridine). ^{1}H NMR ($CDCl_3$): δ = 6.95–7.13 (d, 2H), 7.77–7.88 (m, 2H), 8.08–8.15 (d, 2H), 8.86–8.93 (dd, 2H), 8.97–9.03 (dd, 2H), 10 (OH), 13.5 (s, 1H).

2.3.3 2-(4-(2-Chloroethoxy)phenyl)-1*H*-imidazo[4,5-f] [1,10]phenanthroline, (Phen-Cl)

4-(1-*H*-Imidazo-[4,5-f][1,10]phenanthroline-2-yl)phenol, (phen-OH), and 1-bromo-3-chloropropane (0.032 g, 8.3 mmol) were dissolved in 10 mL DMF and K_2CO_3 was added in that solution. The reaction was performed under reflux for 24 h. After cooling to room temperature 50 mL water was added in to the mixture and filtrated. Then washed with water and recrystallized. FT-IR (cm^{-1}): 3450 (NH), 1670 (C=N), 1080 (C–O), 770 (N–H), 650 (C–Cl). ^{1}H-NMR (DMSO-d6), δ =: 8 − 7 ppm (Ar–H), 3.5 ppm (–O–CH_2, t), 3.3 ppm (–CH_2, m), 3.1 ppm (–CH_2–Cl, t).

2.3.4 2-(4-Carboxyphenyl)imidazo[4,5-f][1,10] phenanthroline, (Phen-COOH)

1,10-Phenanthroline-5,6-dione (0.21 g, 1 mmol), 4-carboxybenzaldehyde (0.18 g, 1.2 mmol) and ammonium acetate (1.54 g, 20 mmol) were refluxed in glacial acetic acid for 3 h. The yellow solution was then allowed to cool to room temperature. A yellow solid started to precipitate and addition of water afforded more powder. All solid phases were collected and washed thoroughly with water, methanol and ether. FT-IR (cm^{-1}): 3060 (N–H), 1707 (C=O), 1614 (C=N). ^{1}H NMR (DMSO-d6): δ = 14.0 (s, 1H), 13.15 (s,

br, 1H), 9.05 (m, 2H), 8.95 (m, 2H), 8.40 (d, 2H), 8.18 (d, 2H), 7.85 (m, 2H).

2.4 Preparation of Superparamagnetic Iron Oxide, SPION

Fe_3O_4 nanoparticles (SPION) with self-magnetic properties were synthesized by co-precipitation of Fe(II) and Fe(III) ions in an alkaline solution: 1.28 M $FeCl_3$ and 0.64 M $FeSO_4{\cdot}7H_2O$ were mixed vigorously. 25 mL of 1M NaOH solution was then added dropwise into the resulting solution over 40 min and then stirred for 4 h. The reaction was carried out in an N_2 gas atmosphere to prevent further oxidation of the iron salts formed by the addition of NaOH. Finally the precipitate was collected by filtration and washed three times with deionized water and then dried under vacuum. Brown color magnetic Fe_3O_4 nanoparticles were synthesized [25].

2.5 Preparation of (3-Aminopropyl)triethoxysilane, APTES and (3-Chloropropyl)dimethoxy Silane, CPTES Coated Superparamagnetic Iron Oxide Nanoparticles

2.5.1 (SPION)-(3-Chloropropyl)dimethoxysilane, CPTES

Superparamagnetic ironoxide nanoparticles Fe_3O_4, (0.10 g, 0.43 mmol) and (3-chloropropyl)dimethoxysilane (CPTES) (0.085 g, 0.043 mmol) were dissolved in 20 mL methanol and refluxed under N_2 atmosphere for 24 h. Then washed with water and cooled to room temperature and dried under vacuum [26]. FT-IR: 1060 cm^{-1} for Si–O–Si, 701 cm^{-1} for Si–O and 490 cm^{-1} (Fe–O).

2.5.2 (SPION)-(3-Aminopropyl)triethoxysilane, APTES

Superparamagnetic ironoxide nanoparticles Fe_3O_4, (0.03 g, 0.6 mmol) and (3-aminopropyl) triethoxysilane (APTES) (0.038 g, 0.033 mmol) were dissolved in 20 mL methanol and refluxed under N_2 atmosphere for 24 h. Then washed with water and cooled to room temperature and dried under vacuum [27]. FT-IR: 1080 cm^{-1} for Si–O–Si, 703 cm^{-1} for Si–O and 490 cm^{-1} (Fe–O).

2.6 Preparation of Phenanthrimidazole Containing Silica Nanoparticle Derivatives

2.6.1 Phen-O-NP

(SPION)–(CPTES) (0.068 g, 0.093 mmol) and 4-(1*H*-imidazo[4,5-f][1,10]phenanthrolin-2-yl)phenol, **Phen-OH**, (0.1 g, 0.15 mmol) was dissolved in 20 mL of methanol and stirred under N_2 under reflux for 24 h. Magnetic molecule was precipitated and filtered. Then washed with water and dried under vacuum. M.P. > 400 °C, FT-IR (cm^{-1}): 1400 – 1200 (pyridyl), 1060 (Si–O–Si), 701 (Si–O) and 490 (Fe–O). Elemental analysis; calculated (found): C, 39.91 (38.99); H, 2.71 (2.65); N, 8.46 (8.17).

2.7 Phen-NH-NP

(SPION)–(APTES) (0.1 g, 0.18 mmol) and 2-(4-(2-chloroethoxy)phenyl)-1*H*-imidazo[4,5-f][1,10]phenanthroline, **Phen-Cl**, (0.068 g, 0.093 mmol) was dissolved in 20 mL of methanol and stirred under N_2 under reflux for 24 h. Magnetic molecule was precipitated and filtered. Then washed with water and dried under vacuum. M.P. > 400 °C, FT-IR (cm^{-1}): 1400 – 1200 (pyridyl), 1100 (Si–O–Si), 700 (Si–O) and 490 (Fe–O). Elemental analysis; calculated (found): C, 41.64 (40.97); H, 3.77 (3.63); N, 9.71 (9.54).

2.7.1 Phen-CON-NP

(SPION)–(APTES) ligand (0.363 g, 0.18 mmol) and 2-(4-carboxylphenyl)imidazole[4,5-f][1,10]phenanthroline, **Phen-COOH**, (0.034 g, 0.093 mmol) was dissolved in 20 mL of methanol and stirred under N_2 under reflux for 24 h. Magnetic molecule was precipitated and filtered. Then washed with water and dried under vacuum. M.P. > 400 °C, FT-IR (cm^{-1}): 1400 – 1200 (pyridyl), 1000 (Si–O–Si), 700 (Si–O) and 490 (Fe–O). Elemental analysis; calculated (found): C, 40.09 (39.89); H, 2.78 (2.63); N, 10.16 (9.93).

3 Result and Discussion

3.1 Synthetic Route

The aim of our study was to obtain phenanthrimidazole derivated superparamagnetic iron dioxide nanoparticles which was coated by silica shell. The syntheses of the hydroxy-, chloro-, carboxy-ended phenanthrimidazole derivatives were completed by the condensation reaction of 1,10-phenanthroline-5,6-dione with aromatic aldehydes as 4-hydroxybenzaldehyde (and 4-carboxybenzaldehyde) in the presence of ammonium acetate in glacial acetic acid medium. The chloro-substituted phenanthrimidazole compound was synthesized by the reaction of (imidazo[4,5-f][1,10]phenanthroline-2-yl)phenol and 1-bromo-3-chloropropane in DMF solution. (Fig. 1). Then, synthesis of superparamagnetic iron dioxide nanoparticles, SPION, were obtained using co-precipitation of $FeCl_3$ and $FeCl_2$ aqueous salt solutions with NaOH. Then, the synthesis of SPION–APTES/CPTES magnetic nanoparticles were completed by the reaction of SPION and silica compounds (Fig. 2). At the last step, we have performed nanoparticle syntheses with

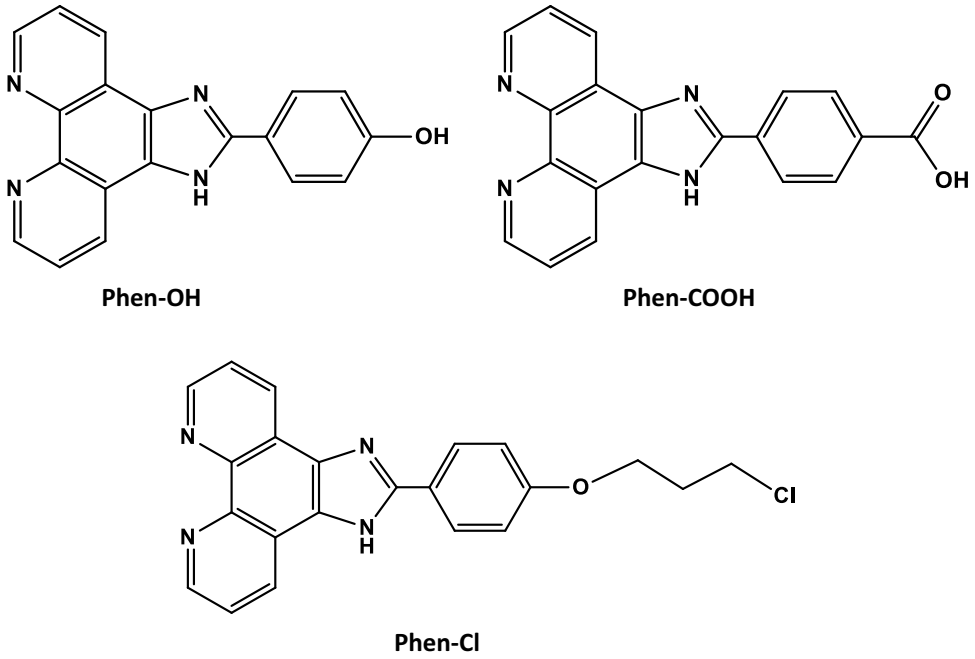

Fig. 1 Phenanthrimidazole-derivated superparamagnetic iron dioxide nanoparticles, Phen-OH, Phen-Cl, Phen-COOH

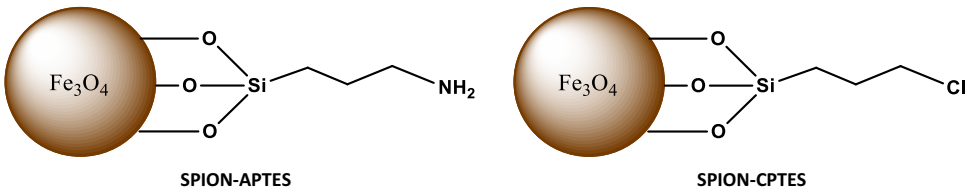

Fig. 2 APTES–SPION and CPTES–SPION magnetic silica shell nanoparticles

phenanthrimidazole derivatives and SPION–APTES/CPTES magnetic silica shells (Fig. 3).

3.2 FT-IR, NMR, Elemental Analyses and TGA/DSC Analyses for the Characterization of the Compounds

The completion of reactions and all the chemical compositions were confirmed by FT-IR spectroscopy, generally. The composition of phenanthrimidazole derivatives also were confirmed by NMR spectroscopy. FT-IR spectra of the phenanthrimidazole-derivative Phen-Cl exhibited strong absorption bands at 3450 cm^{-1} due to NH stretch, 1670 cm^{-1} due to C=N stretch, 1080 cm^{-1} due to C–O stretch, 770 cm^{-1} due to N–H wag and 650 cm^{-1} due to C–Cl stretch. The NMR studies also proved the formation of Phen-Cl molecule with the chemical shifts of δ =: 8 – 7 ppm (Ar–H), 3.5 ppm (–O–CH_2, t), 3.3 ppm (–CH_2, m), 3.1 ppm (–CH_2–Cl, t).

The binding of Fe_3O_4 (SPION) to APTES/CPTES and Phen-X to SPION–APTES/CPTES were confirmed by FT-IR analyses, firstly (Fig. 4). FT-IR spectra of SPION exhibited strong bands in the low frequency region (1000 – 400 cm^{-1}) [28]. The significant peak at 490 cm^{-1} (Fe–O) proved the formation of SPION. For the magnetic silica shells, silica coating over SPION was confirmed by observing the characteristic stretching vibration of Si–O–Si at 1060 cm^{-1} and bending vibration of Si–O band at 701 cm^{-1} for SPION–CPTES and stretching vibration of Si̇–O–Si at 1080 cm^{-1} and bending vibration of Si–O band at 703 cm^{-1} for SPION–APTES.

The phenanthrimidazole-derivated magnetic silica nanoparticles showed specific absorption bands around 1400 – 1200 cm^{-1} due to pyridyl groups, 1000–1100 cm^{-1} due to Si–O–Si stretch, 701–705 cm^{-1} due to Si–O stretch and 490 cm^{-1} due to Fe–O stretch. These results suggested that magnetic silica shells were bonded to phenanthrimidazole derivatives to form final nanoparticles. Figure 4. shows FT-IR spectra of uncoated SPION, silica-coated SPION and silica-coated magnetic nanoparticles, Phen-X-NP for all the nanoparticles. Elemental analyses were performed for the phenanthrimidazole-derivated nanoparticles; for Phen-O-NPs calculated (found): C, 39.91 (38.99); H, 2.71 (2.65); N, 8.46 (8.17), for Phen-NH-NPs calculated (found): C, 41.64 (40.97); H, 3.77 (3.63); N, 9.71 (9.54), and for Phen-CON-NPs calculated (found): C, 40.09 (39.89); H, 2.78 (2.63); N, 10.16 (9.93).

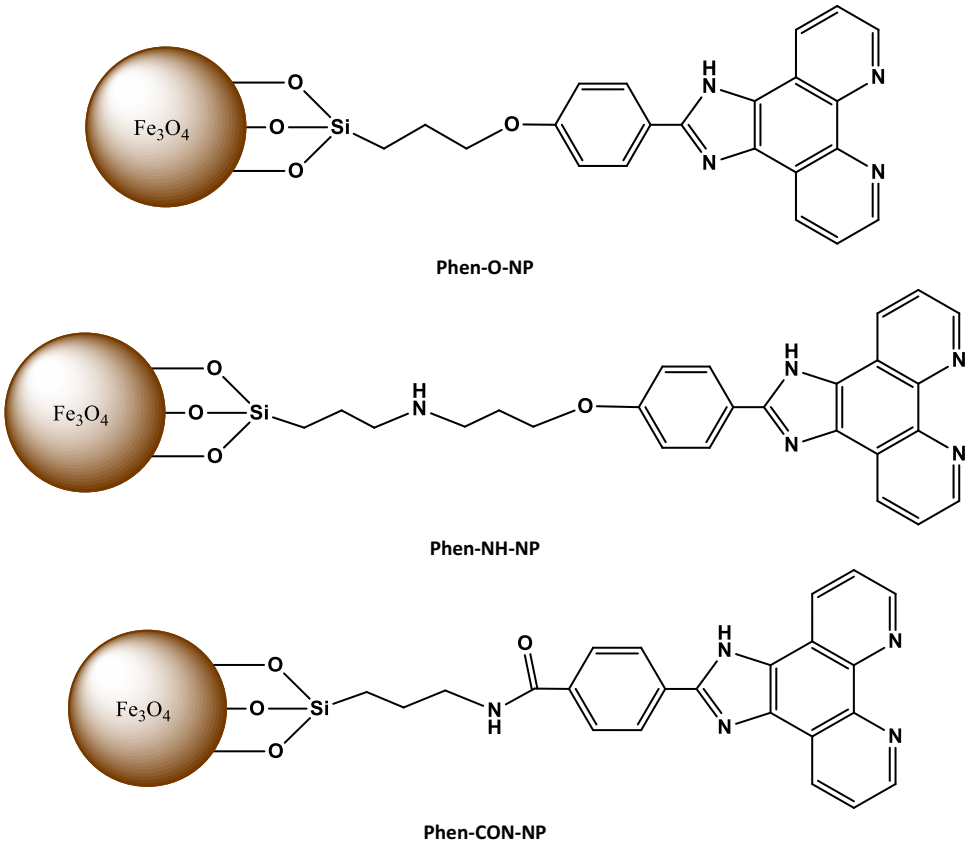

Fig. 3 Phenanthrimidazole-derivated nanoparticles, Phen-O-NP, Phen-NH-NP and Phen-CON-NP

In order to obtain further characterization of the nanoparticles, TGA/DSC thermal analyses were performed. Their plausible degradation schemes are presented in Fig. 5. The thermograms of the phenanthrimidazole-derivated nanoparticles; Phen-O-NP, Phen-NH-NP and Phen-CON-NP, show weight losses at the temperature 40–1000 °C, respectively.

Generally, for all the nanoparticles the weight losses around 100 °C were attributed to the removal of physically adsorbed water, the regions around 250–310 °C were due to removal of coordinated water. The magnetic silica shells SPION–APTES/CPTES thermally decompose nearly at 190–270 °C with sharp weight losses of organic parts and at around 350–440 °C smaller weight losses of the final oxidation of SiO_2. The region between 305 and 458 °C were due to the combustion of amine-bonded parts of phenanthrimidazole group, those not bonded to any the metal group. And the region at 450–900 °C was attributed x to the decomposition of the oxygen-bonded parts of the iron complexes.

The residues were carbon black, some iron oxides and aromatic rings. The observed weight losses for all ligands and complexes are compatible with the calculated values [29].

3.3 X-ray Diffraction (XRD)

The crystal structure of the synthesized magnetic nanoparticles Phen-O-NP, Phen-NH-NP, Phen-CON-NP was characterized by X-ray diffraction (XRD) (Fig. 6). The diffraction peaks at 29°, 36°, 39° and 61° for Phen-O-NP, at 35.5°, 45°, 57° and 63.5° for Phen-NH-NP, 35°, 43°, 58° and 64° for Phen-CON-NP can be assigned to crystal planes of cubic Fe_3O_4, respectively. The broad band which can be observed in range 20°–27° might be ascribed to silica. All above results confirmed that the syntheses procedures of magnetic silica coated nanoparticles. The XRD results indicated that the Phen-O-NP, Phen-NH-NP, Phen-CON-NP hybrid materials contains the crystalline phases of cubic Fe_3O_4 and silica. When we compare the XRD peak intensities of magnetic silica shells (SPION–APTES/CPTES) with phenanthrimidazole-derivated nanoparticles (Phen-O-NP, Phen-NH-NP, Phen-CON-NP), it is obvious that the peak intensities are weaker in Phen-X-NPs. Weakening of the peak intensity is caused by the penetration of the magnetic nanoparticles by the silica and phenanthrimidazole derivated group [30].

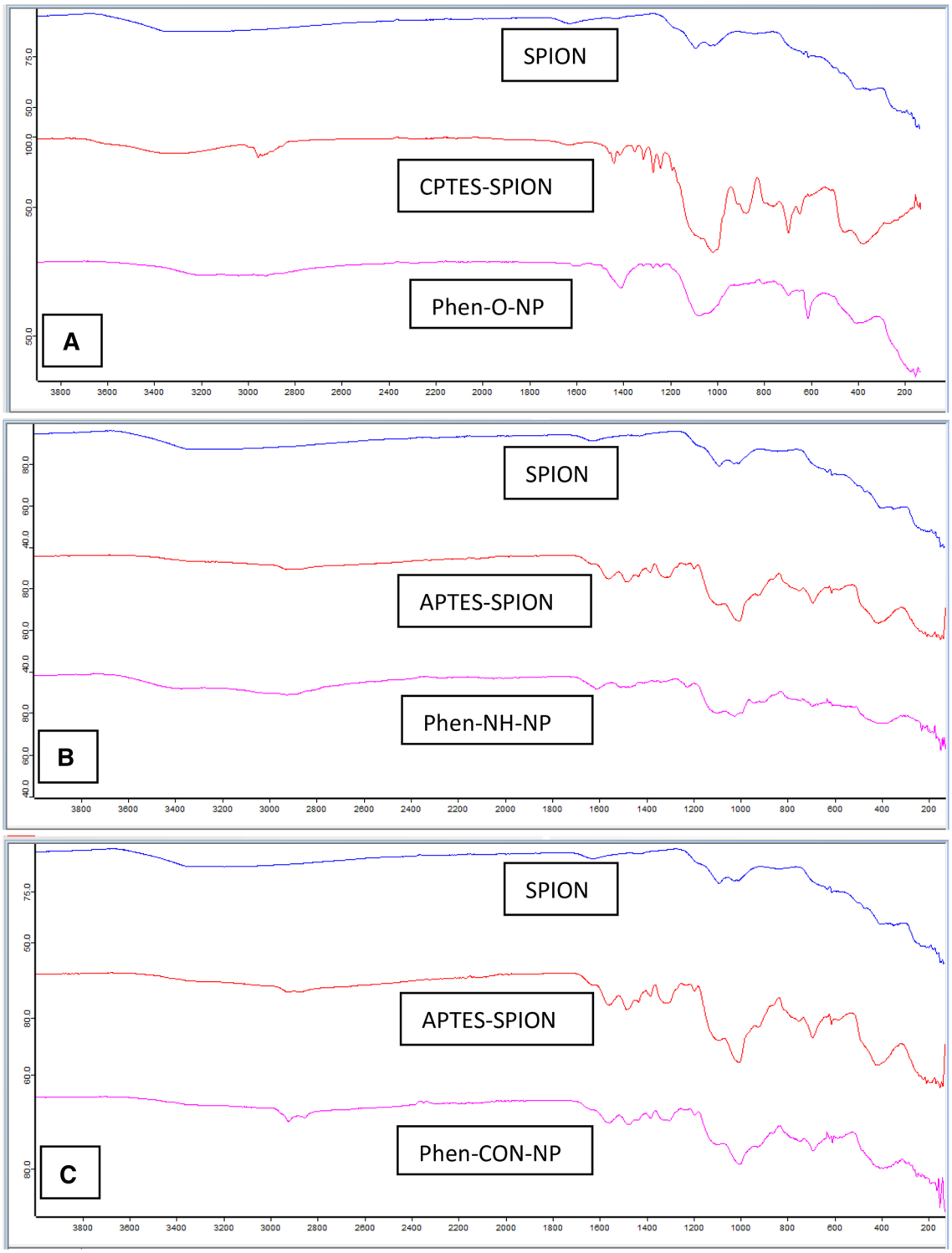

Fig. 4 FT-IR spectra of uncoated SPION, silica-coated SPION and silica-coated magnetic nanoparticles, Phen-X-NP. **a** Spectra of Phen-O-NP group **b** spectra of Phen-NH-NP group and **c** spectra of Phen-CON-NP group

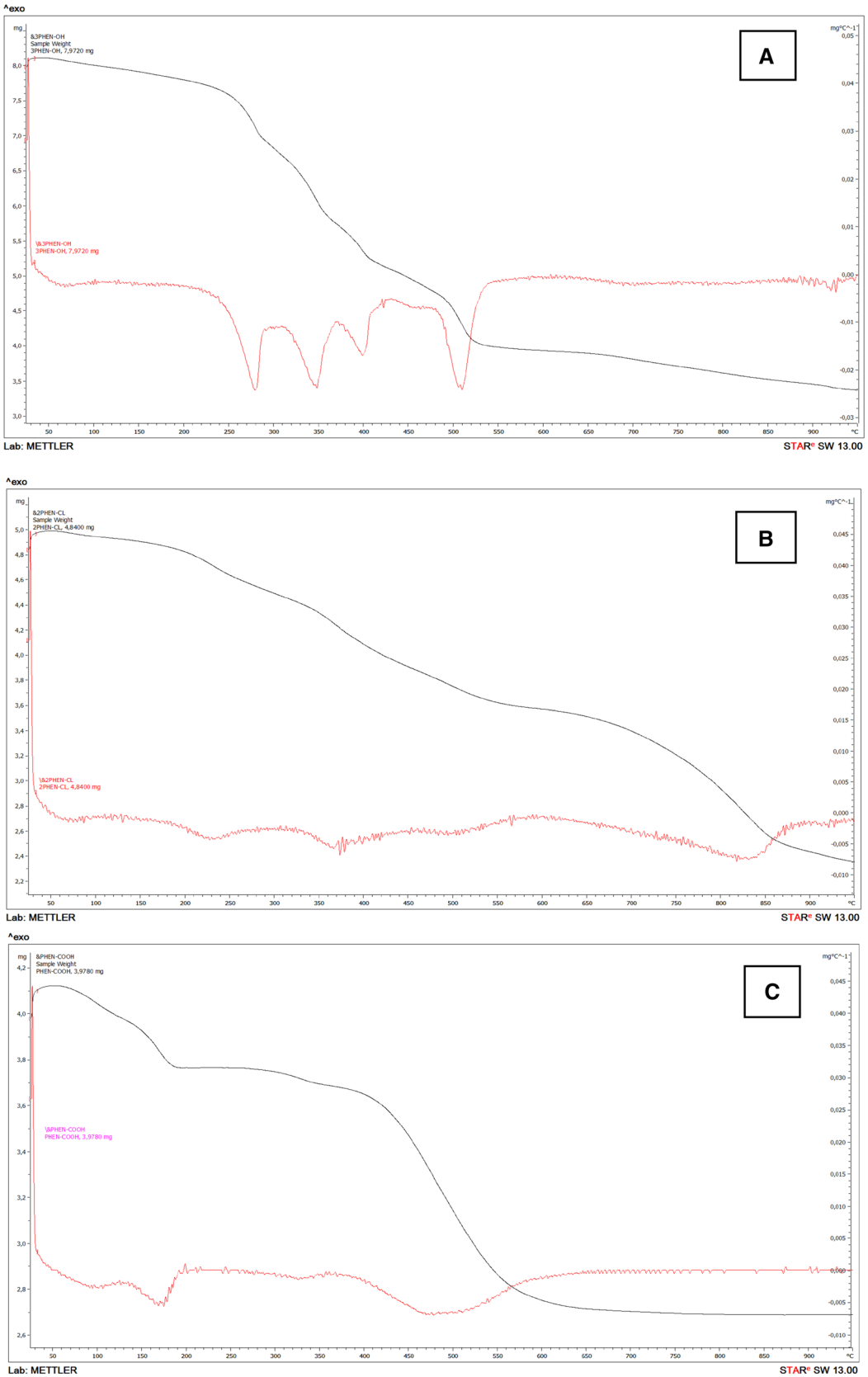

Fig. 5 Thermogravimetric analyses diagrams of the phenanthrimidazole derivated magnetic silica nanoparticles; **a** Phen-O-NP, **b** Phen-NH-NP and **c** Phen-CON-NP nanoparticles

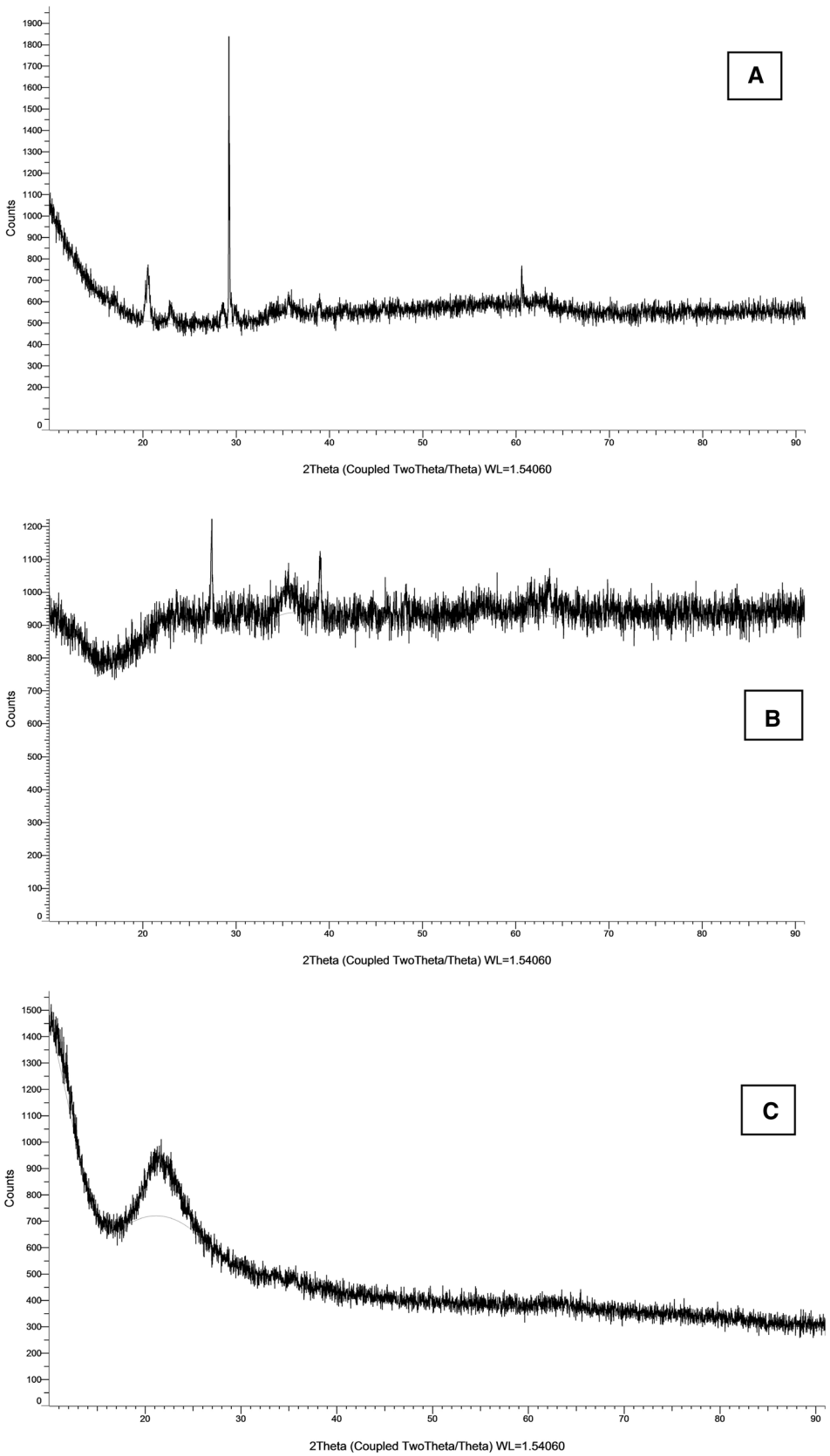

Fig. 6 X-ray diffraction patterns of the phenanthrimidazole derivated magnetic silica nanoparticles; **a** Phen-O-NP, **b** Phen-NH-NP and **c** Phen-CON-NP nanoparticles

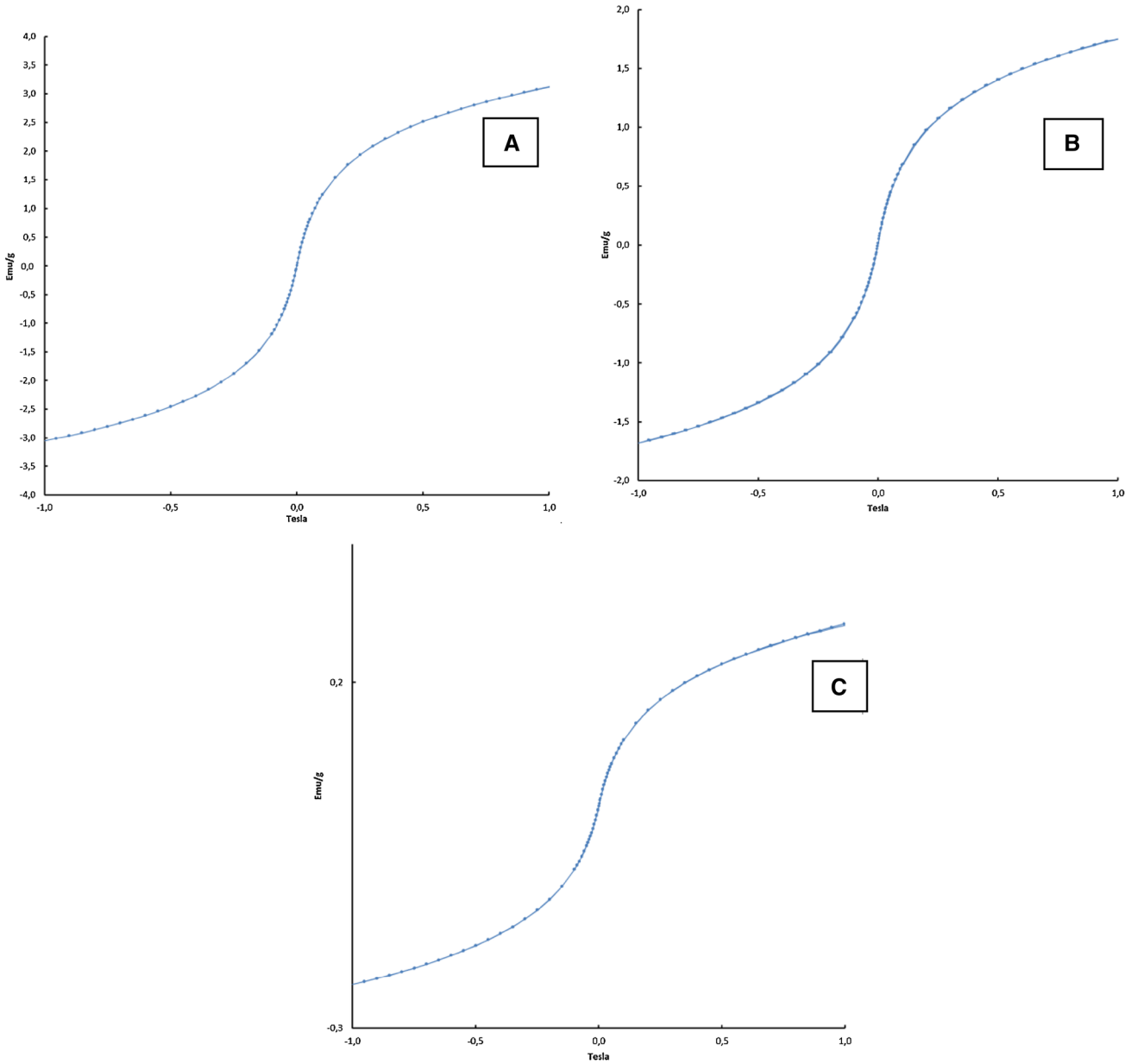

Fig. 7 Magnetization curves in a function of applied magnetic field for the phenanthrimidazole derivated magnetic silica nanoparticles; **a** Phen-O-NP, **b** Phen-NH-NP and **c** Phen-CON-NP by VSM

3.3.1 Magnetization Measurements with VSM and Magnetic Susceptibility

The magnetic properties of the phenanthrimidazole-derivated magnetic silica nanoparticles (Phen-O-NP, Phen-NH-NP, Phen-CON-NP) were studied on solid samples at room temperature by vibrating sample magnetometer (VSM). Saturation magnetization is the most important parameter in VSM studies. Figure 7 presents magnetization curves of nanoparticles and it can be seen that the curves have symmetrical s-shapes and there are no hysteresis observed. Additionally, the material do exhibit saturation behaviour and reached the saturation magnetization values as Ms = 3.1 emu/g for Phen-O-NP, 1.75 emu/g for Phen-NH-NP and 0.3 emu/g for Phen-CON-NP. Generally, it is known that the magnetization of SPION and superparamagnetic silica shells have reached the saturation magnetization. And, it has been also known that coating of magnetic particles with non-magnetic materials like silica or organic layer can decrease the saturation of magnetization [1, 31]. So, the saturation magnetization values of our nanoparticles are smaller than SPION itself.

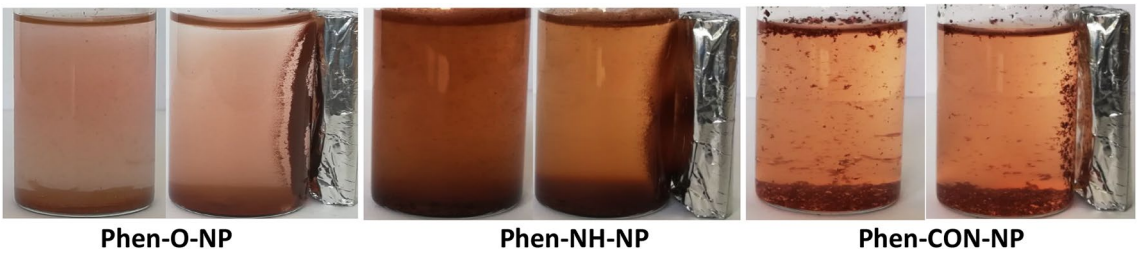

Fig. 8 Dispersion of phenanthrimidazole derivated magnetic nanoparticle samples in ethanol–water mixture (1:1) and in the presence of external magnet

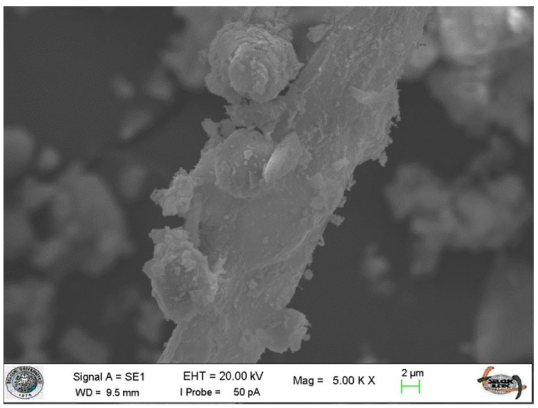

Fig. 9 SEM image of Phen-Cl phenanthrimidazole

Investigations into the magnetic properties of SPION containing molecules continued with the measuring and calculating the magnetic moments by using a magnetic susceptibility device at 300 K. The SPION, itself, is the mixture of FeO and Fe_2O_3. And, the theoretical magnetic moment of Fe^{3+} of Fe_2O_3 maghemite is calculated theoretically as 5.9 BM. SPION containing Phenanthrimidazole-derivated nanoparticles show paramagnetic properties with the magnetic moment values of $\mu_{eff}=4.33$ BM for Phen-O-NP, $\mu_{eff}=4.52$ BM for Phen-NH-NP and $\mu_{eff}=4.47$ BM for Phen-CON-NP.

Figure 8 shows magnetic dispersions of magnetic nanoparticle samples in ethanol–water mixture. As can be seen, Phen-O-NP and Phen-NH-NP were well dispersed in water/ethanol (50/50) mixture. Phen-CON-NP was aggregated at the top and bottom of the mixture. It was also observed that the final magnetic nanoparticles are highly responsive to external magnetic field, so they can be potentially applicable as an MRI enhancement agent.

3.3.2 SEM and TEM Analyses

Scanning electron microscopy (SEM) studies were performed for screening the morphology of the phenanthrimidazole groups, generally. They have long pipe like shapes. Figure 9 shows SEM micrographs for the Phen-Cl molecule.

The main morphologies of the phenanthrimidazole derivated magnetic nanoparticles were screened by transmission electron microscopy (TEM). From the TEM images of the previous studies, it is seen that the shapes of SPION was spherical and aggregated which was due to magnetism of SPION [25, 32]. As we see from the images of final phenanthrimidazole derivated magnetic nanoparticles the shapes were also spherical and aggregated (Fig. 10).

4 Conclusions

The hydroxy-, chloro-, carboxy-ended phenanthrimidazole derivatives were designed to give reaction with SPION-APTES/CPTES magnetic silica nanoparticles. The characterization of chemical compositions were performed by FT-IR, ^{1}H-NMR spectroscopy, TGA/DSC and XRD measurements. The morphologies and magnetic measurements of the magnetic nanoparticles were evaluated by SEM, TEM and VSM magnetometers. The morphological studies show that the resulting products are spherical and aggregated. Their superparamagnetic properties were decreased by the silica coating between SPION and phenanthrimidazole group.

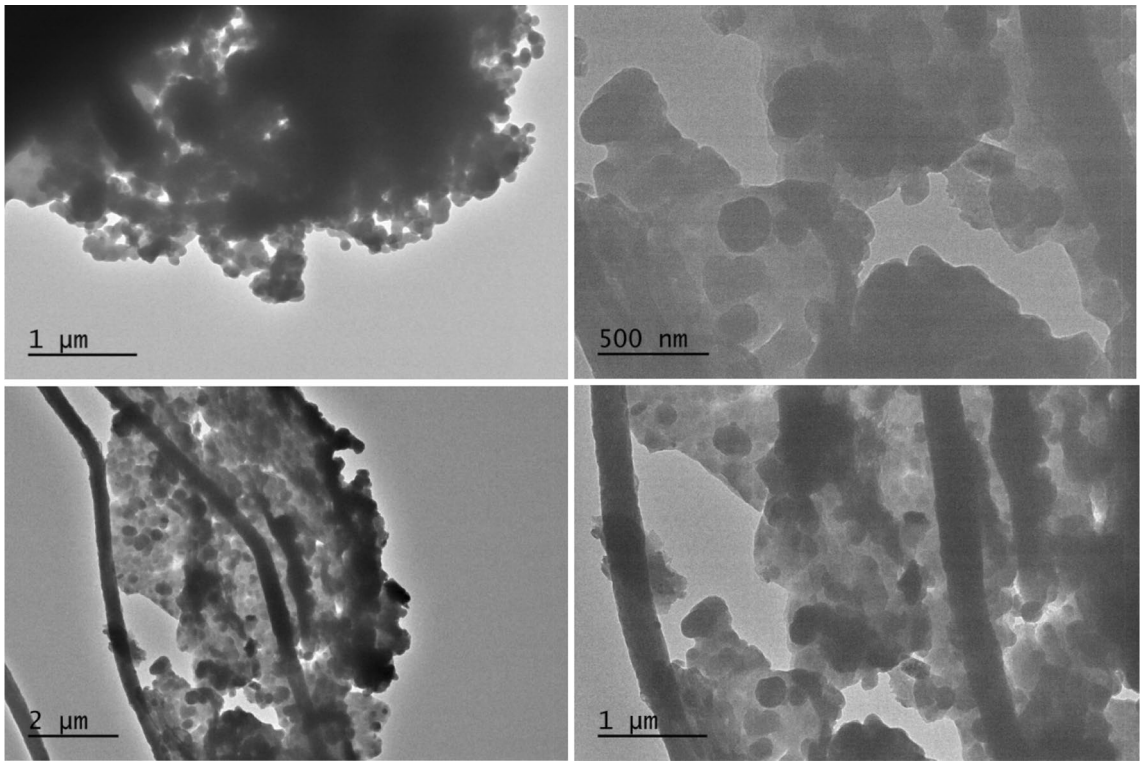

Fig. 10 TEM images of **a** Phen-NH-NP and **b** Phen-O-NP silica coated magnetic nanoparticles. **c**, **d** TEM images of Phen-CON-NP nanoparticles

Acknowledgements We thank the Scientific Research Projects Foundation (BAP) of Selcuk University (Konya/TURKEY) for financial support of this work.

References

1. M.-J. Li, Z. Chen, V.W.-W. Yam, Y. Zu, ACS Nano **2**(5), 905–912 (2008)
2. A. Zelenakova, J. Kovac, V. Zelenak, J. Appl. Phys. **108**(3), 034323 (2010)
3. Z. Lu, G. Wang, J. Zhuang, W. Yang, Colloids Surf. A **278**, 140–143 (2006)
4. S. Uysal, Z.E. Koç, J. Mol. Struct. **1109**, 119–126 (2016)
5. M. Mahmoud, S. Sant, B. Wang, S. Laurent, T. Sen, Adv. Drug Deliv. Rev. **63**, 24–46 (2011)
6. A. Akbarzadeh, M. Samiei, S. Davaran. Nanoscale Res. Lett. **7**, 144 (2012)
7. Z. Xu, Q. Liu, J.A. Finch, Appl. Surf. Sci. **120**, 269 (1997)
8. X. Liu, J. Xing, Y. Guan, Colloids Surf. **238**, 127 (2004)
9. F. Sevgi, U. Bagkesici, A.N. Kursunlu, E. Guler, J. Mol. Struct. **1154**, 256–260 (2018)
10. A.Y. Obal, H.I. Uçan, J. Fluoresc. **25**, 647–655 (2015)
11. P.F. Zhang, Z.C. Chen, Synthesis **2001**, 2075–2077 (2001)
12. G. Chelucci, D. Addis, S. Baldino, Tetrahedron Lett. **48**, 3359 (2007)
13. S. Gladiali, L. Pinna, G. Delogu, E. Graf, H. Brunner, Tetrahedron **1**, 937 (1990)
14. J.M. Plummer, J.A. Weitgenant, B.C. Noll, J.W. Lauher, O. Wiest, P. Helquist, J. Org. Chem. **73**, 3911–3914 (2008)
15. W.Z. Antkowiak, A. Sobczak, Tetrahedron **57**, 2799–2805 (2001)
16. L. Nagarapu, S. Apuri, S. Kantevari, J. Mol. Catal. A **266**, 104–108 (2007)
17. F.C. Krebs, H. Spanggaard, J. Org. Chem. **67**, 7185–7192 (2002)
18. J. Liu, W. Zheng, S. Shi, C. Tan, J. Chen, K. Zheng, L. Ji, J. Inorg. Biochem. **102**, 193 (2008)
19. C. Baslak, Res. Chem. Intermed. (2018). https://doi.org/10.1007/s11164-018-3615-6
20. S. Çelikbilek, Z.E. Koç, J. Mol. Struct. **1065**, 205–209 (2014)
21. A.N. Kursunlu, E. Güler, J. Mol. Struct. **1134**, 345–349 (2017)
22. P. Lenaerts, A. Storms, J. Mullens, J. D'Haen, C. Görller-Walrand, K. Binnemans, K. Driesen, Chem. Mater. **17**, 5194–5201 (2005)
23. A.Y. Obal, H.I. Uçan, J. Fluoresc. **26**, 1685–1697 (2016)
24. Y. Pellegrin, R.J. Forster, T.E. Keyes, Inorg. Chim. Acta **362**, 1715–1722 (2009)
25. A.K. Gupta, M. Gupta, Biomaterials **26**, 3995–4021 (2005)
26. E. Woo, K.M. Ponvel, I.S. Ahn, C.H. Lee, J. Mater. Chem. **20**, 1511–1515 (2010)
27. E. Tamyurek, E. Maltas, S.Z. Bas, M. Ozmen, S. Yildiz. Int. J. Biol. Macromol. **73**, 76–83 (2015)
28. H.L. Ma, X.R. Qi, Y. Maitani, T. Nagai, Int. J. Pharm. **333**, 177–186 (2007)
29. S. Campel, D. Makovec, M. Drofenik, J. Magn. Magn. Mater. **321**, 1346–1350 (2009)
30. J. Lewandowska-Lancucka, M. Staszewska, M. Szuwarzynski, M. Kepczynski, M. Romek, W. Tokarz, A. Szpak, G. Kania, M. Nowakowska. J. Alloy. Compd. **586**, 45–51 (2014)
31. S.R. Kandiband, N. Gundeboin, S. Das, V.M. Sunkara, J. Photochem. Photobiol. B **178**, 270–276 (2018)
32. S. Benyakhou, A. Belmokhtar, A. Zehhaf, A. Benyoucef, J. Mol. Struct. **1150**, 580–585 (2017)